A model and numerical method for compressible flows with capillary effects

Kevin Schmidmayer, Fabien Petitpas, Eric Daniel, Nicolas Favrie, Sergey Gavrilyuk

A model and numerical method for compressible flows with capillary effects

Kevin Schmidmayer[a,*], Fabien Petitpas[a], Eric Daniel[a], Nicolas Favrie[a], Sergey Gavrilyuk[a]

[a] *Aix-Marseille Université, CNRS UMR 7343 IUSTI, 5 rue Enrico Fermi, 13453 Marseille Cedex 13, France*

Abstract

A new model for interface problems and capillary effects in compressible fluids is presented together with a specific numerical method to treat capillary flows and pressure waves propagation. This new model is in agreement with physical principles of conservation, respects the second law of thermodynamics and is shown hyperbolic in a 3D framework. A new numerical method is also proposed where the global system of equations is split into several submodels. Each submodel is hyperbolic and can be solved with an adequate numerical method. This method is tested and validated thanks to comparisons with analytical solutions (Laplace law) and with experimental results on the first stage of droplet breakup induced by a shock wave.

Keywords: Diffuse interface, Godunov type methods, Hyperbolic systems, Multiphase flows, Shock waves, Surface tension

1. Introduction

The breakup of liquid droplets induced by high speed flows has a wide range of engineering and scientific applications and has given rise to a large literature. In some cases, this phenomenon causes damages as for example when droplets are impacting aircrafts in supersonic flight causing erosion of its surface (Engel [8], Joseph *et al.* [20], Igra and Takayama [17, 18]). Studying of droplets behavior in a high speed flow may also be encountered when security issues are considered as for example for shock wave attenuation (Chauvin *et al.* [4, 5]). Other applications can be found in explosive science or in combustion systems where a liquid jet is atomized (Welch and Boyle [41], Meng and Colonius [25], Devassy *et al.* [7]). Detail reviews of droplet breakup study can be found in Pilch and Erdman [33], Wierzba and Takayama [42], Hsiang and Faeth [16].

Regarding numerical simulations, the existing studies of breakup are focused on the first stage of droplet deformation when Richtmyer-Meshkov instability appears (Yang *et al.* [44],

*Corresponding author

Email addresses: kevin.schmidmayer@univ-amu.fr (Kevin Schmidmayer), fabien.petitpas@univ-amu.fr (Fabien Petitpas), eric.daniel@univ-amu.fr (Eric Daniel), nicolas.favrie@univ-amu.fr (Nicolas Favrie), sergey.gavrilyuk@univ-amu.fr (Sergey Gavrilyuk)

Quirk and Karni [34], Layes and Le Metayer [22], Meng and Colonius [25]). Nevertheless, there is no mathematical model capable to treat the effect of the flow on the droplet from the short time scale when the shock wave interacts with the droplet to the long time scale when capillary and/or viscous effects become significant.

In last decades, several studies have been performed taking into account capillary effects in multiphase flow models. The seminal work of Brackbill *et al.* [3] succeeded in transforming a surface force into a volume force, quite easy to treat as a source term in a multiphase flow model. The surface tension volume force is expressed thanks to a color function $\tilde{c}(\mathbf{x})$. This approach has been used in Chen and Doolen [6], Sussman *et al.* [39], Gueyffier *et al.* [15], Osher and Fedkiw [28, 29], Tryggvason *et al.* [40], Perigaud and Saurel [30], Le Martelot *et al.* [23] where capillary effects are added to the momentum and the energy equations.

The aim of this work is to develop a mathematical model and a numerical method for compressible multiphase flows with capillary effects which are conservative, hyperbolic and verifies the entropy inequality.

Section 2 presents Brackbill *et al.* [3] method to treat the surface tension and a review of existing models with a conservative form of the capillary effects. In Section 3, the new conservative model with capillary effects is presented. The model is in agreement with conservation principles and with the second law of thermodynamics. A special attention is paid to the study of hyperbolicity of the model. Section 4 is devoted to the building of a numerical method able to solve capillary terms in a conservative manner. The method is based on split models that are separately hyperbolic. These submodels are solved thanks to adequate numerical schemes. Section 5 presents the validation of the method on 2D test cases. It shows that the model and the numerical method are able to treat accurately both capillary effects and shock wave propagation. Quantitative comparisons are done with other methods based on source terms integration to show the importance of the conservative formulation. The first stage of the aerodynamic breakup of a water column induced by a shock wave is compared with experiments. In Appendix, the model derivation is given.

2. Compressible two-phase capillary flows: state of art

2.1. Surface tension force and color function

The main difficulty in modeling the capillary effects is about considering a surface force in numerical models that solve volume average quantities. The seminal work of Brackbill *et al.* [3], called CSF (Continuum Surface Force) method, succeeded to do it by using a color function, $\tilde{c}(\mathbf{x})$. Thanks to this function, the surface tension volume force is then expressed:

$$\mathbf{F}_v(\mathbf{x}) = \sigma\kappa(\mathbf{x})\frac{\boldsymbol{\nabla}\tilde{c}(\mathbf{x})}{[\tilde{c}]},$$

where σ is the surface tension coefficient and $\kappa(\mathbf{x})$ the local curvature of the interface defined by:

$$\kappa(\mathbf{x}) = -\boldsymbol{\nabla}.\mathbf{n}(\mathbf{x}),$$

with $\mathbf{n}(\mathbf{x})$ is the normal vector to the interface between the both phases:

$$\mathbf{n}(\mathbf{x}) = \frac{\boldsymbol{\nabla}\tilde{c}(\mathbf{x})}{\|\boldsymbol{\nabla}\tilde{c}(\mathbf{x})\|}.$$

The color function $\tilde{c}(\mathbf{x})$ allows us to locate the different fluids and the interface. $\tilde{c}(\mathbf{x})$ is defined as:

$$\tilde{c}(\mathbf{x}) = \begin{cases} c_1 & in \quad fluid \quad 1, \\ c_2 & in \quad fluid \quad 2, \\ c_1 \leqslant \tilde{c}(\mathbf{x}) \leqslant c_2 & in \quad the \quad transition \quad region. \end{cases} \tag{1}$$

In the transition region $\tilde{c}(\mathbf{x})$ is given by an interpolation, meaning that the interface has a non zero thickness. $[\tilde{c}] = c_2 - c_1$ is the jump of the color function.

It is assumed that the color function obeys a transport equation [3]:

$$\frac{\partial \tilde{c}(\mathbf{x})}{\partial t} + \mathbf{u}_I.\boldsymbol{\nabla}\tilde{c}(\mathbf{x}) = 0,$$

where $\mathbf{u}_I$ is the interface velocity.

Numerical results using this force can be found in [6, 23, 28, 29, 39, 40]. In these references, the surface tension force is treated as source terms in the momentum and the energy equations.

2.2. Review of existing compressible models with capillary effects

Because it is the only class of methods able to deal with dynamic appearance and disappearance of interfaces, we focus here on diffuse interface modeling (Abgrall and Karni [1], Saurel and Abgrall [35]). Moreover, this is also the only class of models where the thermodynamics of mixture cells is well defined, thanks to a specific equation of state for each phase (liquid or gas).

The study of capillary effects within the framework of the diffuse interface methods is based on the generalization of the Allaire *et al.* [2] model. This model originally does not include capillary effects. Second law of thermodynamics is verified only if the condition of thermal equilibrium $T = T_k$, with $k = \{1, 2\}$, is retained. Perigaud and Saurel [30] extended this model by including the capillary effects. As a result, the surface tension volume force appears as a flux term in the momentum equation as well as the work of this force $\mathbf{F}_v(\mathbf{x}).\mathbf{u}$ in the total energy equation. In this reference, as Gueyffier *et al.* [15] did within the incompressible flows framework, a conservative formulation was obtained:

$$\begin{cases} \frac{\partial \alpha_1}{\partial t} + \mathbf{u}.\boldsymbol{\nabla}\alpha_1 & = 0, \\ \frac{\partial \alpha_k \rho_k}{\partial t} + \boldsymbol{\nabla}.(\alpha_k \rho_k \mathbf{u}) & = 0, \\ \frac{\partial \rho \mathbf{u}}{\partial t} + \boldsymbol{\nabla}.\left(\rho \mathbf{u} \otimes \mathbf{u} + P\overline{\overline{I}} - \sigma\left(\|\boldsymbol{\nabla}\alpha_1\|\overline{\overline{I}} - \frac{\boldsymbol{\nabla}\alpha_1 \otimes \boldsymbol{\nabla}\alpha_1}{\|\boldsymbol{\nabla}\alpha_1\|}\right)\right) & = 0, \\ \frac{\partial \rho E + \varepsilon_\sigma}{\partial t} + \boldsymbol{\nabla}.\left(\mathbf{u}(\rho E + \varepsilon_\sigma + P) - \sigma\left(\|\boldsymbol{\nabla}\alpha_1\|\overline{\overline{I}} - \frac{\boldsymbol{\nabla}\alpha_1 \otimes \boldsymbol{\nabla}\alpha_1}{\|\boldsymbol{\nabla}\alpha_1\|}\right).\mathbf{u}\right) & = 0, \end{cases}$$

where α_k and ρ_k are the volume fraction and the density of phase k. ρ, $\mathbf{u}$, P, $E = e + \frac{1}{2}\|\mathbf{u}\|^2$ and e are respectively the mixture variables for density, velocity, pressure, total energy and

internal energy. The mixture internal energy is defined as $e = \sum_k Y_k e_k(\rho_k, P)$ and each fluid is governed by its own convex equation of state (EOS) $e_k = e_k(\rho_k, P)$. Introducing the capillary effects in fluxes (conservative formulation) leads to a new term in the mixture total energy equation, $\varepsilon_\sigma = \sigma\|\boldsymbol{\nabla}\alpha_1\|$ which is defined as a capillary potential energy. Note that α_1 obeys a transport equation and plays the role of the color function (1) because $\mathbf{u}_I = \mathbf{u}$ when the velocity equilibrium is considered. In [30], the authors used a pressure equilibrium closure, allowing the resolution of interface problems dedicated to high speed flows. Nevertheless, this closure does not allow to have conservation law for the mixture entropy.

Le Martelot *et al.* [23] corrected this drawback by including the capillary effects in a velocity, pressure and temperature equilibrium system of equations by considering the mass fraction as the color function: the second law of thermodynamics is then respected because of the thermal equilibrium closure. Such a closure is reasonable for the description of the boiling phenomenon, but this thermal equilibrium is too drastic for breakup droplet study under high speed flows what is the main subject of this paper.

It becomes then obvious that the establishment of a new model with the capillary effects in conservative form that can still preserve the mixture entropy law without the temperature equilibrium hypothesis is necessary. The model should also be well posed (in particular, hyperbolic) to guarantee the numerical treatment of physical problems.

3. Mechanical equilibrium model with capillary effects

3.1. The model

The new model we will propose here is able to treat breakup of droplet study under high speed flows and respects the second law of thermodynamics. It is based on the Kapila *et al.* basic system of equations [21]. This last model has been shown to be suitable to treat interface problems between compressible fluids. Multiple extensions of this model have been developped to solve several concrete problems dealing with phase transition (Massoni *et al.* [24], Saurel *et al.* [37], cavitation (Petitpas *et al.* [31]), detonation in high energetic materials (Petitpas *et al.* [32]), solid-fluid interaction and compaction of granular media (Favrie and Gavrilyuk [10, 9]) and low Mach number flows (Murrone and Guillard [26]). It considers compressible two-phase flows in mechanical equilibrium (pressure and velocity equilibrium). In this model, the volume fraction obeys the following equation:

$$\frac{\partial \alpha_1}{\partial t} + \mathbf{u}.\boldsymbol{\nabla}\alpha_1 = K\boldsymbol{\nabla}.\mathbf{u}, \tag{2}$$

where the term $K\boldsymbol{\nabla}.\mathbf{u}$ accounts for the differences in the acoustic behaviour of both phases. It traduces pressure equilibrium between phases. K is given by:

$$K = \frac{\rho_2 a_2^2 - \rho_1 a_1^2}{\frac{\rho_2 a_2^2}{\alpha_2} + \frac{\rho_1 a_1^2}{\alpha_1}},$$

a_k being the sound of speed of phase k.

The capillary effects are then added in conservative form. Because the color function is purely a geometric variable, a supplementary equation for the color function is added. Applying the Hamilton principle for the model derivation (see Appendix for details), the model becomes:

$$\begin{cases} \frac{\partial \alpha_1}{\partial t} + \mathbf{u}.\boldsymbol{\nabla}\alpha_1 - K\boldsymbol{\nabla}.\mathbf{u} & = 0, \\ \frac{\partial \alpha_k \rho_k}{\partial t} + \boldsymbol{\nabla}.\left(\alpha_k \rho_k \mathbf{u}\right) & = 0, \\ \frac{\partial \rho \mathbf{u}}{\partial t} + \boldsymbol{\nabla}.\left(\rho \mathbf{u} \otimes \mathbf{u} + P\overline{\overline{I}} + \overline{\overline{\Omega}}\right) & = 0, \\ \frac{\partial \rho E + \varepsilon_\sigma}{\partial t} + \boldsymbol{\nabla}.\left(\left(\rho E + \varepsilon_\sigma + P\right)\mathbf{u} + \overline{\overline{\Omega}}.\mathbf{u}\right) & = 0, \\ \frac{\partial c}{\partial t} + \mathbf{u}.\boldsymbol{\nabla} c & = 0, \end{cases} \tag{3}$$

with $\overline{\overline{\Omega}}$ being the capillary tensor given by:

$$\overline{\overline{\Omega}} = -\sigma\left(\|\boldsymbol{\nabla} c\|\overline{\overline{I}} - \frac{\boldsymbol{\nabla} c \otimes \boldsymbol{\nabla} c}{\|\boldsymbol{\nabla} c\|}\right). \tag{4}$$

The capillary energy is equal to $\varepsilon_\sigma = \sigma\|\boldsymbol{\nabla} c\|$ and the color function is normalized by its jump $c = \tilde{c}/[\tilde{c}]$.

The surface tension terms do not affect the pressure and the entropy equations. The pressure equation evolution then reads:

$$\frac{dP}{dt} + \rho a^2 \boldsymbol{\nabla}.\left(\mathbf{u}\right) = 0.$$

where a is the Wood mixture speed of sound [43]:

$$a^2 = \left(\rho \sum_k \frac{\alpha_k}{\rho_k a_k^2}\right)^{-1}.$$

As in Kapila *et al.* [21], the entropy equations remain unchanged in continuous motion:

$$\frac{ds_k}{dt} = 0,$$

with the material derivative operator $d(\cdot)/dt = \partial(\cdot)/\partial t + \mathbf{u}.\boldsymbol{\nabla}(\cdot)$. The mixture entropy is obviously assured:

$$\frac{ds}{dt} = \sum_k \frac{dY_k s_k}{dt} = 0.$$

3.2. Hyperbolicity

In this chapter, the study of the hyperbolicity of system (3) is done. Thanks to the rotational invariance of the equations, the study can be reduced to the study of the only x-direction in the 3D system of equations.

3.2.1. Primitive form

First, the model needs to be transformed into a vector form:

$$\frac{\partial \mathbf{W}}{\partial t} + \overline{\overline{A}}(\mathbf{W}) \frac{\partial \mathbf{W}}{\partial x} = 0. \tag{5}$$

The color function is first rewritten by taking its gradient to obtain a conservative equation for $\mathbf{w} = \boldsymbol{\nabla} c$:

$$\frac{\partial \mathbf{w}}{\partial t} + \boldsymbol{\nabla} (\mathbf{u}.\mathbf{w}) = 0.$$

Or, in an equivalent form:

$$\frac{\partial \mathbf{w}}{\partial t} + \left(\frac{\partial \mathbf{w}}{\partial \mathbf{x}}\right)^T .\mathbf{u} + \left(\frac{\partial \mathbf{u}}{\partial \mathbf{x}}\right)^T .\mathbf{w} = 0. \tag{6}$$

Since $\mathbf{w}$ is a gradient, we have:

$$rot(\mathbf{w}) = \mathbf{0}, \tag{7}$$

i.e.

$$\left(\frac{\partial \mathbf{w}}{\partial \mathbf{x}}\right)^T = \left(\frac{\partial \mathbf{w}}{\partial \mathbf{x}}\right).$$

Thus, equation (6) with the constraint (7) becomes:

$$\frac{\partial \mathbf{w}}{\partial t} + \left(\frac{\partial \mathbf{w}}{\partial \mathbf{x}}\right).\mathbf{u} + \left(\frac{\partial \mathbf{u}}{\partial \mathbf{x}}\right)^T .\mathbf{w} = \mathbf{0}. \tag{8}$$

Constraint (7) also appears in solid mechanics where the formulation of the extended system under a "*rot*" constraint is important in the hyperbolicity study (see Ndanou *et al.* [27]). Equation (8) may be developed in three dimensions, where we denote $\mathbf{u} = (u, v, w)^T$, $\mathbf{w} = (w_1, w_2, w_3)^T$ and $\mathbf{x} = (x, y, z)^T$:

$$\left\{\begin{array}{ll} \frac{\partial w_1}{\partial t} + \frac{\partial w_1}{\partial x}u + \frac{\partial w_1}{\partial y}v + \frac{\partial w_1}{\partial z}w + \frac{\partial u}{\partial x}w_1 + \frac{\partial v}{\partial x}w_2 + \frac{\partial w}{\partial x}w_3 & = 0, \\ \frac{\partial w_2}{\partial t} + \frac{\partial w_2}{\partial x}u + \frac{\partial w_2}{\partial y}v + \frac{\partial w_2}{\partial z}w + \frac{\partial u}{\partial y}w_1 + \frac{\partial v}{\partial y}w_2 + \frac{\partial w}{\partial y}w_3 & = 0, \\ \frac{\partial w_3}{\partial t} + \frac{\partial w_3}{\partial x}u + \frac{\partial w_3}{\partial y}v + \frac{\partial w_3}{\partial z}w + \frac{\partial u}{\partial z}w_1 + \frac{\partial v}{\partial z}w_2 + \frac{\partial w}{\partial z}w_3 & = 0. \end{array}\right. \tag{9}$$

In the case where all the variables depend only on (t, x), (9) reduces to:

$$\left\{\begin{array}{ll} \frac{\partial w_1}{\partial t} + \frac{\partial w_1}{\partial x}u + \frac{\partial u}{\partial x}w_1 + \frac{\partial v}{\partial x}w_2 + \frac{\partial w}{\partial x}w_3 & = 0, \\ \frac{\partial w_2}{\partial t} + \frac{\partial w_2}{\partial x}u & = 0, \\ \frac{\partial w_3}{\partial t} + \frac{\partial w_3}{\partial x}u & = 0. \end{array}\right.$$

Introduction of the vector $\mathbf{w}$ allows us to rewrite components for the capillary tensor $\overline{\overline{\Omega}}$ (4) in the x-direction:

$$\Omega_{11} = \sigma \left(\frac{-w_2^2 - w_3^2}{\sqrt{w_1^2 + w_2^2 + w_3^2}}\right),$$

$$\Omega_{12} = \sigma\left(\frac{w_1 w_2}{\sqrt{w_1^2+w_2^2+w_3^2}}\right),$$

$$\Omega_{13} = \sigma\left(\frac{w_1 w_3}{\sqrt{w_1^2+w_2^2+w_3^2}}\right).$$

Finally, the system rewritten in vector form reads for two phases:

$$\begin{cases}
\frac{\partial \alpha_1}{\partial t} + u\frac{\partial \alpha_1}{\partial x} - K\frac{\partial u}{\partial x} & = 0,\\
\frac{\partial u}{\partial t} + u\frac{\partial u}{\partial x} + \frac{1}{\rho}\left(\frac{\partial P}{\partial x} + \frac{\partial \Omega_{11}}{\partial w_1}\frac{\partial w_1}{\partial x} + \frac{\partial \Omega_{11}}{\partial w_2}\frac{\partial w_2}{\partial x} + \frac{\partial \Omega_{11}}{\partial w_3}\frac{\partial w_3}{\partial x}\right) & = 0,\\
\frac{\partial v}{\partial t} + u\frac{\partial v}{\partial x} + \frac{1}{\rho}\left(\frac{\partial \Omega_{12}}{\partial w_1}\frac{\partial w_1}{\partial x} + \frac{\partial \Omega_{12}}{\partial w_2}\frac{\partial w_2}{\partial x} + \frac{\partial \Omega_{12}}{\partial w_3}\frac{\partial w_3}{\partial x}\right) & = 0,\\
\frac{\partial w}{\partial t} + u\frac{\partial w}{\partial x} + \frac{1}{\rho}\left(\frac{\partial \Omega_{13}}{\partial w_1}\frac{\partial w_1}{\partial x} + \frac{\partial \Omega_{13}}{\partial w_2}\frac{\partial w_2}{\partial x} + \frac{\partial \Omega_{13}}{\partial w_3}\frac{\partial w_3}{\partial x}\right) & = 0,\\
\frac{\partial P}{\partial t} + u\frac{\partial P}{\partial x} + \rho a^2\frac{\partial u}{\partial x} & = 0,\\
\frac{\partial w_1}{\partial t} + u\frac{\partial w_1}{\partial x} + w_1\frac{\partial u}{\partial x} + w_2\frac{\partial v}{\partial x} + w_3\frac{\partial w}{\partial x} & = 0,\\
\frac{\partial w_2}{\partial t} + u\frac{\partial w_2}{\partial x} & = 0,\\
\frac{\partial w_3}{\partial t} + u\frac{\partial w_3}{\partial x} & = 0,\\
\frac{\partial s_1}{\partial t} + u\frac{\partial s_1}{\partial x} & = 0,\\
\frac{\partial s_2}{\partial t} + u\frac{\partial s_2}{\partial x} & = 0,\\
\frac{\partial Y_1}{\partial t} + u\frac{\partial Y_1}{\partial x} & = 0.\\
\frac{\partial c}{\partial t} + u\frac{\partial c}{\partial x} & = 0
\end{cases}$$

3.2.2. Eigenvalues

The vector $\mathbf{W}$ and the matrix $\overline{\overline{A}}$ in (5) are then defined by:

$$\mathbf{W} = [\alpha_1, u, v, w, P, w_1, w_2, w_3, s_1, s_2, Y_1, c]^T$$

$$\overline{\overline{A}}(\mathbf{W}) = \begin{bmatrix}
u & -K & 0 & 0 & 0 & 0 & 0 & 0 & 0 & 0 & 0 & 0\\
0 & u & 0 & 0 & \frac{1}{\rho} & \frac{1}{\rho}\frac{\partial \Omega_{11}}{\partial w_1} & \frac{1}{\rho}\frac{\partial \Omega_{11}}{\partial w_2} & \frac{1}{\rho}\frac{\partial \Omega_{11}}{\partial w_3} & 0 & 0 & 0 & 0\\
0 & 0 & u & 0 & 0 & \frac{1}{\rho}\frac{\partial \Omega_{12}}{\partial w_1} & \frac{1}{\rho}\frac{\partial \Omega_{12}}{\partial w_2} & \frac{1}{\rho}\frac{\partial \Omega_{12}}{\partial w_3} & 0 & 0 & 0 & 0\\
0 & 0 & 0 & u & 0 & \frac{1}{\rho}\frac{\partial \Omega_{13}}{\partial w_1} & \frac{1}{\rho}\frac{\partial \Omega_{13}}{\partial w_2} & \frac{1}{\rho}\frac{\partial \Omega_{13}}{\partial w_3} & 0 & 0 & 0 & 0\\
0 & \rho a^2 & 0 & 0 & u & 0 & 0 & 0 & 0 & 0 & 0 & 0\\
0 & w_1 & w_2 & w_3 & 0 & u & 0 & 0 & 0 & 0 & 0 & 0\\
0 & 0 & 0 & 0 & 0 & 0 & u & 0 & 0 & 0 & 0 & 0\\
0 & 0 & 0 & 0 & 0 & 0 & 0 & u & 0 & 0 & 0 & 0\\
0 & 0 & 0 & 0 & 0 & 0 & 0 & 0 & u & 0 & 0 & 0\\
0 & 0 & 0 & 0 & 0 & 0 & 0 & 0 & 0 & u & 0 & 0\\
0 & 0 & 0 & 0 & 0 & 0 & 0 & 0 & 0 & 0 & u & 0\\
0 & 0 & 0 & 0 & 0 & 0 & 0 & 0 & 0 & 0 & 0 & u
\end{bmatrix}$$

The determinant of matrix $\overline{\overline{A}}$ can be calculated:

$$\det\left(\overline{\overline{A}}(\mathbf{W}) - \lambda\overline{\overline{I}}\right) = (u-\lambda)^8\left[(u-\lambda)^4 + L(u-\lambda)^2 + M\right],$$

where:

$$L = -a^2 - \frac{1}{\rho}\left(w_1\frac{\partial\Omega_{11}}{\partial w_1} + w_2\frac{\partial\Omega_{12}}{\partial w_1} + w_3\frac{\partial\Omega_{13}}{\partial w_1}\right),$$

$$M = \frac{a^2}{\rho}\left(w_2\frac{\partial\Omega_{12}}{\partial w_1} + w_3\frac{\partial\Omega_{13}}{\partial w_1}\right).$$

8 real eigenvalues are straightforward found:

$$\lambda_{1,2,3,4,5,6,7,8} = u.$$

The 4 other eigenvalues are the roots of the quadratic equation:

$$X^2 + LX + M = 0, \tag{10}$$

with $X = (u-\lambda)^2$. If the discriminant Δ is positive, the roots of equation (10) are real and complex numbers otherwise. That condition determines if the system is hyperbolic or not. Defining the components of the normal vector $n_k = w_k/\left\|\mathbf{w}\right\|$, after some calculations the discriminant is:

$$\Delta = \left(a^2 + \frac{\sigma\|\mathbf{w}\|}{\rho}\left(n_2^2+n_3^2\right)\right)^2 - 4a^2\frac{\sigma\|\mathbf{w}\|}{\rho}\left(n_2^2+n_3^2\right)^2.$$

But:

$$\left(n_2^2+n_3^2\right) \leqslant 1.$$

Hence:

$$\begin{aligned}\Delta &\geqslant \left(a^2 + \frac{\sigma\|\mathbf{w}\|}{\rho}\left(n_2^2+n_3^2\right)\right)^2 - 4a^2\frac{\sigma\|\mathbf{w}\|}{\rho}\left(n_2^2+n_3^2\right)\\ &= \left(a^2 - \frac{\sigma\|\mathbf{w}\|}{\rho}\left(n_2^2+n_3^2\right)\right)^2 \geqslant 0.\end{aligned}$$

The roots of the quadratic equation (10) are then all real. Thus, the corresponding eigenvalues of model (3) are real, explicit and given by:

$$\lambda_{9,10} = u \pm a_s, \tag{11}$$

$$\lambda_{11,12} = u \pm a_c, \tag{12}$$

where:

$$a_s = \frac{a^2+b+\sqrt{\left(a^2+b\right)^2 - 4a^2b\left(n_2^2+n_3^2\right)}}{2},$$

$$a_c = \frac{a^2+b-\sqrt{\left(a^2+b\right)^2 - 4a^2b\left(n_2^2+n_3^2\right)}}{2},$$

and:

$$b = \frac{\sigma\|\mathbf{w}\|}{\rho}\left(n_2^2+n_3^2\right).$$

Finally, there are 8 multiple eigenvalues $\lambda = u$ and 4 eigenvalues corresponding to sound waves (equation (11)) and capillary waves (equation (12)) ordered as:

$$u - a_s < u - a_c \leqslant u \leqslant u + a_c < u + a_s.$$

The system is hyperbolic if the multiple eigenvalues $\lambda = u$ has exactly 8 linearly independent eigenvectors. This is the case, so the system is hyperbolic. The whole system of the eigenvectors will not be given because this equilibrium system will not be numerically solved in this form (see Section 4 for discussion).

4. Numerical resolution of model (3)

4.1. Basic ideas

The numerical solution of model (3) represents a challenge regarding the two following points :

- The first difficulty is due to the $K\boldsymbol{\nabla}.\mathbf{u}$ term in the volume fraction evolution equation. This is the precious ingredient leading to the respect of the mixture entropy equation when a pressure equilibrium assumption is retained. Nevertheless, the presence of this non-conservative term considerably complicates the numerical method which crucially depends on the choice of appropriate Rankine-Hugoniot relations (see [13] and [38] for details). This is a reason why a non-equilibrium pressure model is preferred with a pressure relaxation term instead of the non-conservative term $K\boldsymbol{\nabla}.\mathbf{u}$ in the volume fraction equation. This model is presented in this section.

- The second difficulty is in the simultaneous treatment of 5 waves which are present in the model. This difficulty is circumvented by the use of split models that are proven to be hyperbolic separately.

4.1.1. A pressure relaxation model with capillary effects

Because the non-conservative volume fraction equation represents a major problem regarding numerical resolution, the following non-equilibrium pressure hyperbolic model is proposed:

$$\left\{\begin{array}{ll}
\frac{\partial \alpha_1}{\partial t} + \mathbf{u}.\nabla\alpha_1 & = \mu\left(P_1 - P_2\right), \\
\frac{\partial \alpha_1\rho_1}{\partial t} + \boldsymbol{\nabla}.\left(\alpha_1\rho_1\mathbf{u}\right) & = 0, \\
\frac{\partial \alpha_2\rho_2}{\partial t} + \boldsymbol{\nabla}.\left(\alpha_2\rho_2\mathbf{u}\right) & = 0, \\
\frac{\partial \rho\mathbf{u}}{\partial t} + \boldsymbol{\nabla}.\left(\rho\mathbf{u}\otimes\mathbf{u} + P\overline{\overline{I}} + \overline{\overline{\Omega}}\right) & = \mathbf{0}, \\
\frac{\partial \alpha_1\rho_1 e_1}{\partial t} + \boldsymbol{\nabla}.\left(\alpha_1\rho_1 e_1\mathbf{u}\right) + \alpha_1 P_1\boldsymbol{\nabla}.\mathbf{u} & = -\mu P_I\left(P_1 - P_2\right), \\
\frac{\partial \alpha_2\rho_2 e_2}{\partial t} + \boldsymbol{\nabla}.\left(\alpha_2\rho_2 e_2\mathbf{u}\right) + \alpha_2 P_2\boldsymbol{\nabla}.\mathbf{u} & = \mu P_I\left(P_1 - P_2\right), \\
\frac{\partial c}{\partial t} + \mathbf{u}.\boldsymbol{\nabla}c & = 0,
\end{array}\right. \tag{13}$$

where μ is the pressure relaxation coefficient, $P_I = \frac{Z_2P_1 + Z_1P_2}{Z_1 + Z_2}$ (see [36] for details) and $Z_k = \rho_k c_k$ represents the acoustic impedance of the phase k. The mixture pressure is given by:

$$P = \alpha_1 P_1 + \alpha_2 P_2.$$

Due to the condition $P_1 \neq P_2$ in this model, the total energy equation of the mixture is replaced by the internal energy equation for each phase. Nevertheless, the mixture total energy equation of the system can be written in usual form:

$$\frac{\partial \rho E + \varepsilon_\sigma}{\partial t} + \boldsymbol{\nabla}. \left((\rho E + \varepsilon_\sigma + P) \, \mathbf{u} + \overline{\overline{\Omega}}.\mathbf{u} \right) = 0. \tag{14}$$

The equation (14) is redundant when both internal energy equations are solved, but it will appear to be an important ingredient for numerical method to ensure the energy conservation and to preserve a correct treatment of shock waves.

The hyperbolicity study for model (13) can be done in the same way that for model (3). The model is shown hyperbolic.

One can note that the surface tension effects are missing in the phasic energy equations since it is only a mixture characteristic.

The entropy equations for system (13) can also be written:

$$\alpha_1 \rho_1 T_1 \frac{ds_1}{dt} = \mu (P_1 - P_2)^2 \frac{Z_1}{Z_1 + Z_2},$$

$$\alpha_2 \rho_2 T_2 \frac{ds_2}{dt} = \mu (P_1 - P_2)^2 \frac{Z_2}{Z_1 + Z_2},$$

that insures the mixture entropy ($s = Y_1 s_1 + Y_2 s_2$) increasing.

Model (3) can be recovered as asymptotic limit of model (13) when the pressure of phases tends to be equal. Nevertheless, even if this model is also hyperbolic, it is not a good candidate regarding numerical resolution as mentioned previously. A special splitting procedure will be done for a numerical resolution of model (13).

4.1.2. Splitting procedure

Model (13) without the relaxation terms is split in two submodels. The first submodel does not take into account the surface tension terms. The hyperbolicity is then easily verified. The second submodel contains the only capillary terms and is also proven hyperbolic. Such an approach was also used in Favrie *et al.* [11] where the splitting procedure was used to separate the treatment of longitudinal and shear waves in hyperelasticity.

Hyperbolic submodel 1

The first submodel is similar to that presented in [38] with an additional equation for the color function:

$$\begin{cases} \dfrac{\partial \alpha_1}{\partial t} + \mathbf{u}.\boldsymbol{\nabla}\alpha_1 & = 0, \\ \dfrac{\partial \alpha_1\rho_1}{\partial t} + \boldsymbol{\nabla}.(\alpha_1\rho_1\mathbf{u}) & = 0, \\ \dfrac{\partial \alpha_2\rho_2}{\partial t} + \boldsymbol{\nabla}.(\alpha_2\rho_2\mathbf{u}) & = 0, \\ \dfrac{\partial \rho\mathbf{u}}{\partial t} + \boldsymbol{\nabla}.\left(\rho\mathbf{u}\otimes\mathbf{u} + P\overline{\overline{I}}\right) & = \mathbf{0}, \\ \dfrac{\partial \alpha_1\rho_1 e_1}{\partial t} + \boldsymbol{\nabla}.(\alpha_1\rho_1 e_1\mathbf{u}) + \alpha_1 P_1\boldsymbol{\nabla}.\mathbf{u} & = 0, \\ \dfrac{\partial \alpha_2\rho_2 e_2}{\partial t} + \boldsymbol{\nabla}.(\alpha_2\rho_2 e_2\mathbf{u}) + \alpha_2 P_2\boldsymbol{\nabla}.\mathbf{u} & = 0, \\ \dfrac{\partial c}{\partial t} + \mathbf{u}.\boldsymbol{\nabla}c & = 0. \end{cases} \tag{15}$$

Model (15) may be rewritten in a vector form (5) with:

$$\mathbf{W} = [\alpha_1, s_1, s_2, u, v, w, P_1, P_2, c]^T$$

$$\overline{\overline{A}}(\mathbf{W}) = \begin{bmatrix} u & 0 & 0 & 0 & 0 & 0 & 0 & 0 & 0 \\ 0 & u & 0 & 0 & 0 & 0 & 0 & 0 & 0 \\ 0 & 0 & u & 0 & 0 & 0 & 0 & 0 & 0 \\ \frac{P_1-P_2}{\rho} & 0 & 0 & u & 0 & 0 & \frac{\alpha_1}{\rho} & \frac{\alpha_2}{\rho} & 0 \\ 0 & 0 & 0 & 0 & u & 0 & 0 & 0 & 0 \\ 0 & 0 & 0 & 0 & 0 & u & 0 & 0 & 0 \\ 0 & 0 & 0 & \rho_1 a_1^2 & 0 & 0 & u & 0 & 0 \\ 0 & 0 & 0 & \rho_2 a_2^2 & 0 & 0 & 0 & u & 0 \\ 0 & 0 & 0 & 0 & 0 & 0 & 0 & 0 & u \end{bmatrix}$$

The eigenvalues of the system are:

$$\lambda_{1,2,3,4,5,6,7} = u,$$

$$\lambda_8 = u - a_f,$$

$$\lambda_9 = u + a_f,$$

where a_f is the frozen mixture sound speed:

$$a_f^2 = Y_1 a_1^2 + Y_2 a_2^2.$$

The hyperbolicity of this first submodel is proven in [38].

Hyperbolic submodel 2

The second submodel contains only capillary terms:

$$\begin{cases} \frac{\partial \alpha_1}{\partial t} & = 0, \\ \frac{\partial \alpha_1 \rho_1}{\partial t} & = 0, \\ \frac{\partial \alpha_2 \rho_2}{\partial t} & = 0, \\ \frac{\partial \rho \mathbf{u}}{\partial t} + \boldsymbol{\nabla}.\overline{\overline{\Omega}} & = \mathbf{0}, \\ \frac{\partial \alpha_1 \rho_1 e_1}{\partial t} & = 0, \\ \frac{\partial \alpha_2 \rho_2 e_2}{\partial t} & = 0, \\ \frac{\partial c}{\partial t} & = 0. \end{cases} \tag{16}$$

The system is rewritten in a vector form (5) in the x-direction :

$$\begin{cases} \frac{\partial \alpha_1}{\partial t} & = 0, \\ \frac{\partial s_1}{\partial t} & = 0, \\ \frac{\partial s_2}{\partial t} & = 0, \\ \frac{\partial u}{\partial t} + \frac{1}{\rho}\left(\frac{\partial \Omega_{11}}{\partial w_1}\frac{\partial w_1}{\partial x} + \frac{\partial \Omega_{11}}{\partial w_2}\frac{\partial w_2}{\partial x} + \frac{\partial \Omega_{11}}{\partial w_3}\frac{\partial w_3}{\partial x}\right) & = 0, \\ \frac{\partial v}{\partial t} + \frac{1}{\rho}\left(\frac{\partial \Omega_{12}}{\partial w_1}\frac{\partial w_1}{\partial x} + \frac{\partial \Omega_{12}}{\partial w_2}\frac{\partial w_2}{\partial x} + \frac{\partial \Omega_{12}}{\partial w_3}\frac{\partial w_3}{\partial x}\right) & = 0, \\ \frac{\partial w}{\partial t} + \frac{1}{\rho}\left(\frac{\partial \Omega_{13}}{\partial w_1}\frac{\partial w_1}{\partial x} + \frac{\partial \Omega_{13}}{\partial w_2}\frac{\partial w_2}{\partial x} + \frac{\partial \Omega_{13}}{\partial w_3}\frac{\partial w_3}{\partial x}\right) & = 0, \\ \frac{\partial P_1}{\partial t} & = 0, \\ \frac{\partial P_2}{\partial t} & = 0, \\ \frac{\partial w_1}{\partial t} & = 0, \\ \frac{\partial w_2}{\partial t} & = 0, \\ \frac{\partial w_3}{\partial t} & = 0. \end{cases}$$

The eigenvalues of the system are all real and there are as much linearly independent eigenvectors as eigenvalues. So, the second submodel is also hyperbolic.

Relaxation step

This step is exactly the same as in [38].

4.2. Numerical Method

Finally, the numerical method is presented as a 3-step method. Each step is successively performed in order to circumvent specific numerical problems:

- First, the hyperbolic non-equilibrium pressure model (15) is solved using a Godunov-type method.
- Secondly, model (16) is solved. A specific attention is paid to the choice for the flux terms in order to ensure the momentum and energy conservation.
- Third, a relaxation procedure leads to the pressure equilibrium.

The chain of these three steps is equivalent to solve model (3). Each step of the method is presented in details hereafter. The full system of equations is first rewritten in the following vector form:

$$\frac{\partial \mathbf{U}}{\partial t} + \frac{\partial \left(\mathbf{F}_h^x\left(\mathbf{U}\right) + \mathbf{F}_c^x\left(\mathbf{U}\right)\right)}{\partial x} + \frac{\partial \left(\mathbf{F}_h^y\left(\mathbf{U}\right) + \mathbf{F}_c^y\left(\mathbf{U}\right)\right)}{\partial y} + \frac{\partial \left(\mathbf{F}_h^z\left(\mathbf{U}\right) + \mathbf{F}_c^z\left(\mathbf{U}\right)\right)}{\partial z} + \mathbf{H}_{nc}\boldsymbol{\nabla}.\mathbf{u} = \mathbf{H}_{relax}.$$

The vector $\mathbf{U}$ contains the unknown quantities defined in the system:

$$\mathbf{U} = \left[\alpha_1, \alpha_1\rho_1, \alpha_2\rho_2, \rho u, \rho v, \rho w, \alpha_1\rho_1 e_1, \alpha_2\rho_2 e_2, c, \rho E + \varepsilon_\sigma\right]^T$$

The vectors $\mathbf{F}_h^\beta\left(\mathbf{U}\right)$, $\mathbf{F}_c^\beta\left(\mathbf{U}\right)$, $\mathbf{H}_{nc}$ and $\mathbf{H}_{relax}$, with $\beta = \{x, y, z\}$, contain respectively the hydrodynamic fluxes, the capillary fluxes, the non-conservative terms and the relaxation terms:

$$\mathbf{F}_h^x\left(\mathbf{U}\right) = \begin{bmatrix} \alpha_1 u \\ \alpha_1\rho_1 u \\ \alpha_2\rho_2 u \\ \rho u^2 + P \\ \rho uv \\ \rho uw \\ \alpha_1\rho_1 e_1 u \\ \alpha_2\rho_2 e_2 u \\ cu \\ \left(\rho E + P\right) u \end{bmatrix} \quad \mathbf{F}_h^y\left(\mathbf{U}\right) = \begin{bmatrix} \alpha_1 v \\ \alpha_1\rho_1 v \\ \alpha_2\rho_2 v \\ \rho uv \\ \rho v^2 + P \\ \rho vw \\ \alpha_1\rho_1 e_1 v \\ \alpha_2\rho_2 e_2 v \\ cv \\ \left(\rho E + P\right) v \end{bmatrix} \quad \mathbf{F}_h^z\left(\mathbf{U}\right) = \begin{bmatrix} \alpha_1 w \\ \alpha_1\rho_1 w \\ \alpha_2\rho_2 w \\ \rho uw \\ \rho vw \\ \rho w^2 + P \\ \alpha_1\rho_1 e_1 w \\ \alpha_2\rho_2 e_2 w \\ cw \\ \left(\rho E + P\right) w \end{bmatrix}$$

$$\mathbf{F}_c^x\left(\mathbf{U}\right) = \begin{bmatrix} 0 \\ 0 \\ 0 \\ \Omega_{11} \\ \Omega_{12} \\ \Omega_{13} \\ 0 \\ 0 \\ 0 \\ \varepsilon_\sigma u + \Omega_{11} u + \Omega_{12} v + \Omega_{13} w \end{bmatrix} \quad \mathbf{F}_c^y\left(\mathbf{U}\right) = \begin{bmatrix} 0 \\ 0 \\ 0 \\ \Omega_{21} \\ \Omega_{22} \\ \Omega_{23} \\ 0 \\ 0 \\ 0 \\ \varepsilon_\sigma u + \Omega_{21} u + \Omega_{22} v + \Omega_{23} w \end{bmatrix}$$

$$\mathbf{F}_c^z(\mathbf{U}) = \begin{bmatrix} 0 \\ 0 \\ 0 \\ \Omega_{31} \\ \Omega_{32} \\ \Omega_{33} \\ 0 \\ 0 \\ 0 \\ \varepsilon_\sigma u + \Omega_{31} u + \Omega_{32} v + \Omega_{33} w \end{bmatrix}$$

$$\mathbf{H}_{nc} = \begin{bmatrix} -\alpha_1 \\ 0 \\ 0 \\ 0 \\ 0 \\ \alpha_1 P_1 \\ \alpha_2 P_2 \\ -c \\ 0 \end{bmatrix} \qquad \mathbf{H}_{relax} = \begin{bmatrix} \mu(P_1 - P_2) \\ 0 \\ 0 \\ 0 \\ 0 \\ -\mu P_I (P_1 - P_2) \\ \mu P_I (P_1 - P_2) \\ 0 \\ 0 \end{bmatrix}$$

It is important to note that the additional equation for the mixture total energy has been added to the system for numerical solution purposes. This equation is obviously in agreement with the complete system (13) and will be necessary to correct the energy conservation equation during the final relaxation step.

The unknown vector $\mathbf{U}^{n+1}$ is obtained from the initial condition $\mathbf{U}^n$ by application of the three successive operators according to the sequence:

$$\mathbf{U}^{n+1} = L_{relax} L_{cap} L_{hyper}(\mathbf{U}^n).$$

Each step of the numerical method corresponds to the application of one of the three operators detailed below in a cartesian 2D framework.

4.2.1. Hyperbolic operator

The application of the first operator L_{hyper} corresponds to the solution of the hyperbolic submodel (15) using a Godunov-type method [14] extended to an high-order scheme with a MUSCL-Hancock procedure. The solution for this step is given for the cell (i, j) by:

$$\mathbf{U}_{i,j}^{hyper} = \mathbf{U}_{i,j}^n - \mathbf{G}\Delta t,$$

$$\mathbf{G} = \left\{ \begin{array}{l} \frac{1}{\Delta x}\left(\mathbf{F}^{*}_{h;i+\frac{1}{2},j}\left(\mathbf{U}^{n+\frac{1}{2}}_{i,j,R},\mathbf{U}^{n+\frac{1}{2}}_{i+1,j,L}\right)-\mathbf{F}^{*}_{h;i-\frac{1}{2},j}\left(\mathbf{U}^{n+\frac{1}{2}}_{i-1,j,R},\mathbf{U}^{n+\frac{1}{2}}_{i,j,L}\right)\right) \\ +\frac{1}{\Delta y}\left(\mathbf{F}^{*}_{h;i,j+\frac{1}{2}}\left(\mathbf{U}^{n+\frac{1}{2}}_{i,j,T},\mathbf{U}^{n+\frac{1}{2}}_{i,j+1,B}\right)-\mathbf{F}^{*}_{h;i,j-\frac{1}{2}}\left(\mathbf{U}^{n+\frac{1}{2}}_{i,j-1,T},\mathbf{U}^{n+\frac{1}{2}}_{i,j,B}\right)\right) \\ +\frac{\mathbf{H}^{n}_{nc;i,j}}{\Delta x}\left(u^{*}_{i+\frac{1}{2},j}\left(\mathbf{U}^{n+\frac{1}{2}}_{i,j,R},\mathbf{U}^{n+\frac{1}{2}}_{i+1,j,L}\right)-u^{*}_{i-\frac{1}{2},j}\left(\mathbf{U}^{n+\frac{1}{2}}_{i-1,j,R},\mathbf{U}^{n+\frac{1}{2}}_{i,j,L}\right)\right) \\ +\frac{\mathbf{H}^{n}_{nc;i,j}}{\Delta y}\left(v^{*}_{i,j+\frac{1}{2}}\left(\mathbf{U}^{n+\frac{1}{2}}_{i,j,T},\mathbf{U}^{n+\frac{1}{2}}_{i,j+1,B}\right)-v^{*}_{i,j-\frac{1}{2}}\left(\mathbf{U}^{n+\frac{1}{2}}_{i,j-1,T},\mathbf{U}^{n+\frac{1}{2}}_{i,j,B}\right)\right) \end{array} \right\}.$$

The superscript * represents the solution of the Riemann problem on the corresponding cell boundary using the extrapolated values to the cell boundary $\mathbf{U}^{n+\frac{1}{2}}$ in the case of high order method (the subscripts R, L, T, B represent respectively the right, left, top and bottom neighbouring cells). These fluxes can be computed by any Riemann solver, here a Harten-Lax-van Leer Contact (HLLC) approximate Riemann solver is used. Details of this method can be found in Saurel *et al.* [38]. Since the time marching scheme is explicit, the time step obeys a classical Courant-Friedrichs-Lewy (CFL) criterion.

4.2.2. Capillary operator

The second operator L_{cap} introduces capillary terms and corresponds to the solution of submodel (16):

$$\mathbf{U}^{cap} = L_{cap}\left(\mathbf{U}^{hyper}\right).$$

Application of the operator L_{cap} on vector $\mathbf{U}^{hyper}$ is done in the volume-finite framework:

$$\mathbf{U}^{cap}_{i,j} = \mathbf{U}^{hyper}_{i,j} - \Delta t \left\{ \begin{array}{l} \frac{1}{\Delta x}\left(\mathbf{F}^{x}_{c;i+\frac{1}{2},j}\left(\mathbf{U}^{hyper}_{i+\frac{1}{2},j}\right)-\mathbf{F}^{x}_{c;i-\frac{1}{2},j}\left(\mathbf{U}^{hyper}_{i-\frac{1}{2},j}\right)\right) \\ +\frac{1}{\Delta y}\left(\mathbf{F}^{y}_{c;i,j+\frac{1}{2}}\left(\mathbf{U}^{hyper}_{i,j+\frac{1}{2}}\right)-\mathbf{F}^{y}_{c;i,j-\frac{1}{2}}\left(\mathbf{U}^{hyper}_{i,j-\frac{1}{2}}\right)\right) \end{array} \right\}.$$

Because the only equations affected by the capillary effects are the momentum and the total energy equations, these equations are developed in two dimensions:

$$(\rho u)^{cap}_{i,j} = (\rho u)^{hyper}_{i,j} - \sigma\Delta t \left\{ \begin{array}{c} -\frac{\|\mathbf{w}\|^{hyper}_{i+\frac{1}{2},j}-\|\mathbf{w}\|^{hyper}_{i-\frac{1}{2},j}}{\Delta x}+\frac{\left(\frac{w_1^2}{\|\mathbf{w}\|}\right)^{hyper}_{i+\frac{1}{2},j}-\left(\frac{w_1^2}{\|\mathbf{w}\|}\right)^{hyper}_{i-\frac{1}{2},j}}{\Delta x} \\ +\frac{\left(\frac{w_1 w_2}{\|\mathbf{w}\|}\right)^{hyper}_{i,j+\frac{1}{2}}-\left(\frac{w_1 w_2}{\|\mathbf{w}\|}\right)^{hyper}_{i,j-\frac{1}{2}}}{\Delta y} \end{array} \right\},$$

$$(\rho v)^{cap}_{i,j} = (\rho v)^{hyper}_{i,j} - \sigma\Delta t \left\{ \begin{array}{c} -\frac{\|\mathbf{w}\|^{hyper}_{i,j+\frac{1}{2}}-\|\mathbf{w}\|^{hyper}_{i,j-\frac{1}{2}}}{\Delta y}+\frac{\left(\frac{w_1 w_2}{\|\mathbf{w}\|}\right)^{hyper}_{i+\frac{1}{2},j}-\left(\frac{w_1 w_2}{\|\mathbf{w}\|}\right)^{hyper}_{i-\frac{1}{2},j}}{\Delta x} \\ +\frac{\left(\frac{w_2^2}{\|\mathbf{w}\|}\right)^{hyper}_{i,j+\frac{1}{2}}-\left(\frac{w_2^2}{\|\mathbf{w}\|}\right)^{hyper}_{i,j-\frac{1}{2}}}{\Delta y} \end{array} \right\},$$

and for total energy:

$$(\rho E+\varepsilon_\sigma)^{cap}_{i,j} = (\rho E+\varepsilon_\sigma)^{hyper}_{i,j} - \sigma\Delta t \left\{ \begin{array}{l} \frac{\left(\frac{w_1^2 u}{\|\mathbf{w}\|}\right)^{hyper}_{i+\frac{1}{2},j}-\left(\frac{w_1^2 u}{\|\mathbf{w}\|}\right)^{hyper}_{i-\frac{1}{2},j}}{\Delta x}+\frac{\left(\frac{w_1 w_2 v}{\|\mathbf{w}\|}\right)^{hyper}_{i+\frac{1}{2},j}-\left(\frac{w_1 w_2 v}{\|\mathbf{w}\|}\right)^{hyper}_{i-\frac{1}{2},j}}{\Delta x} \\ +\frac{\left(\frac{w_1 w_2 u}{\|\mathbf{w}\|}\right)^{hyper}_{i,j+\frac{1}{2}}-\left(\frac{w_1 w_2 u}{\|\mathbf{w}\|}\right)^{hyper}_{i,j-\frac{1}{2}}}{\Delta y}+\frac{\left(\frac{w_2^2 v}{\|\mathbf{w}\|}\right)^{hyper}_{i,j+\frac{1}{2}}-\left(\frac{w_2^2 v}{\|\mathbf{w}\|}\right)^{hyper}_{i,j-\frac{1}{2}}}{\Delta y} \end{array} \right\}.$$

The different capillary terms at the cell boundary are obtained by the means of an arithmetic average of quantities of neighbouring cells. The vector $\mathbf{w}$ requires derivatives of the color function which are computed by using second-order finite difference approximations.

4.2.3. Pressure relaxation operator

To go through the operators chain, the solution at time $n+1$ is obtained which corrects the components of $\mathbf{U}^{cap}$ by a pressure relaxation algorithm:

$$\mathbf{U}^{n+1} = L_{relax}\left(\mathbf{U}^{cap}\right).$$

The pressure relaxation details can be found in Saurel *et al.* [38] as well as the correction procedure used to guarantee total energy conservation.

5. Numerical results and validations

In this section, two dimensional test cases are proposed to prove that the model and the numerical method are able to treat accurately both capillary effects and shock wave propagation.

In each presented cases, the equations of state (EOS) for air and water are the same. The air obeys the ideal gas law:

$$P_{air} = \left(\gamma_{air} - 1\right)\rho_{air} e_{air},$$

with $\gamma_{air} = 1.4$.

The water follows the stiffened gas EOS:

$$P_{water} = \left(\gamma_{water} - 1\right)\rho_{water} e_{water} - \gamma_{water} P_{\infty,water}.$$

The stiffened gas EOS parameters are $\gamma_{water} = 2.1$ and $P_{\infty,water} = 6.10^6 Pa$.

5.1. Validation of capillary effects

2D tests are proposed to study the ability of the method to treat accurately capillary effects. The proposed method described in the present paper is compared with previous existing methods that use source terms integration. A particular attention is paid to the convergence, the numerical stability, the conservative property, the accuracy with respect with the Laplace pressure law and the dynamics of capillary flows. It is showed that the use of the present method is fully justified to simulate capillary effects in presence of pressure waves. We denote in the following "conservative method" as the numerical method of Section 4 to distinguish it from the source terms integration methods that do not conserve neither the momentum nor the energy.

The first test case consists in solving a cylindrical column of water (2D water droplet) placed in air. The initial density in air is equal to 1 $kg.m^{-3}$ and 1000 $kg.m^{-3}$ in the water. The radius of the water column is set to 0.15m and the surface tension coefficient is equal to $800N.m^{-1}$. These unrealistic values are chosen to magnify the model properties. The

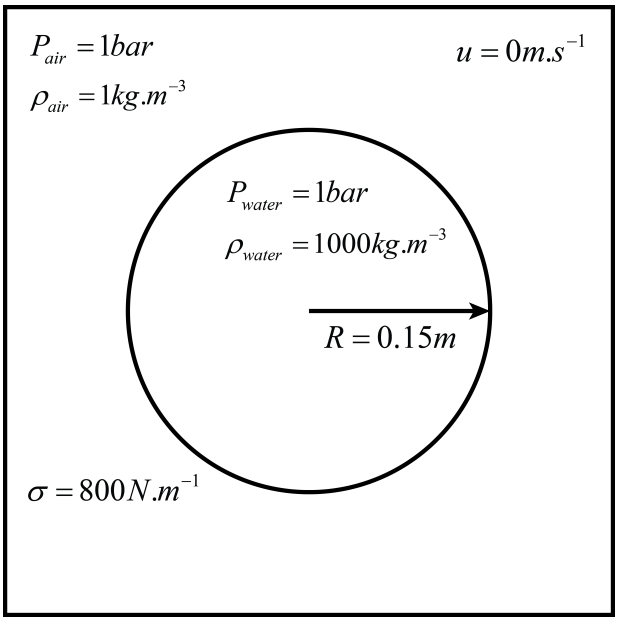

Figure 1: Sketch of initial conditions for simulations of a cylindrical water column (2D water droplet).

pressure is initially uniform in the whole domain and set to 1 *bar* (the initial conditions are presented in Figure 1).

2D computations are performed on the cartesian mesh containing 120x120 computational cells for a physical domain of $75cm$ x $75cm$. Outgoing pressure wave boundary conditions are used. It consists on imposing the Neumann boundary conditions for the pressure and imposing in-outgoing conditions expressed in terms of the Riemann invariants.

5.1.1. Convergence

Because of capillary effects, the pressure of the water column converges to satisfy the Laplace law. Pressure convergence is analyzed using the relative residual:

$$\epsilon = Max\left(\frac{|P_{i,j}^n - P_{i,j}^{n-1}|}{P_{i,j}^n}\right).$$

The convergence is considered to be reached when the criterion $\epsilon \leqslant 1.10^{-4}$ is verified. Evolution of this relative residual is presented in Figure 2 for the proposed conservative method and compared with the source terms integration method of capillary terms. We observe that the pressure convergence is much faster using the conservative method than using the source terms integration one. Moreover, the computational time needed to reach the same physical time with the two different methods is almost the same (a maximum difference of 5% of the computational time is observed). So, the conservative method is definitely faster.

5.1.2. Stability

Regarding the stability of the method, contours of the water column are presented in Figure 3. On the left of this figure the initial contour is shown together with the mesh. Effect

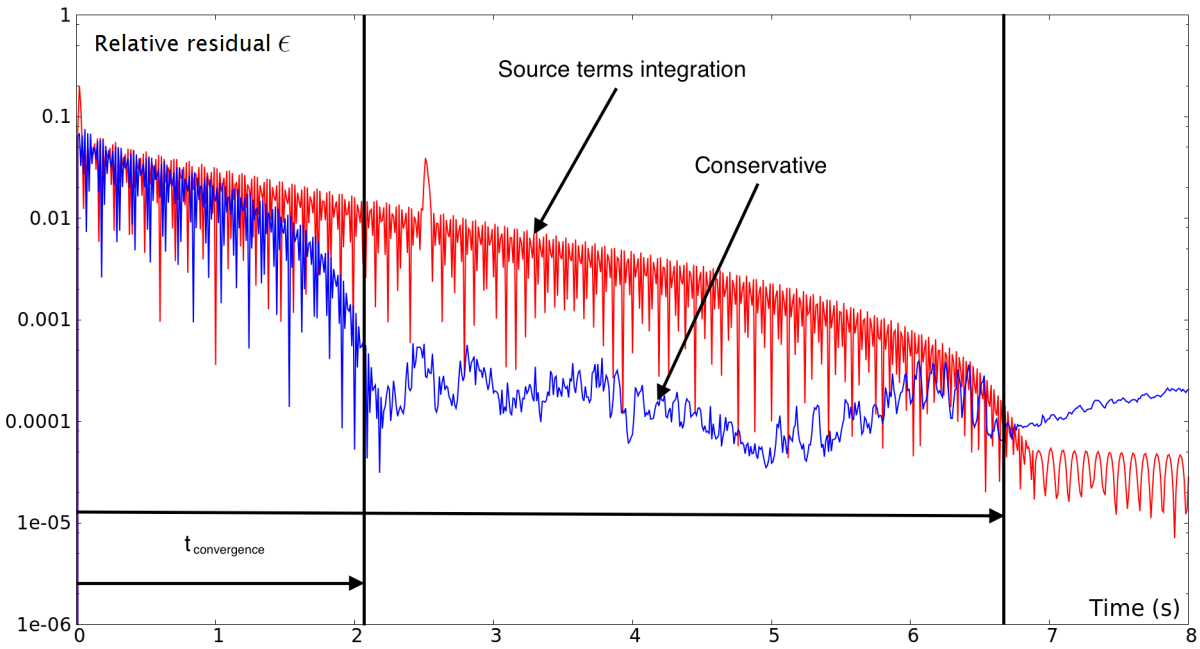

Figure 2: Relative residual ϵ function of physical time for 2D water column test case. Source terms integration (red) and conservative (blue) methods. Convergence is reached after 2 seconds with the proposed conservative method compared to more than 6 seconds with the source terms integration one.

of the mesh on the initial circle is noticeable. The two other figures show contours position immediately after the convergence is reached for both conservative and non-conservative methods. It clearly appears that the source terms integration method of the capillary effects is less stable than the conservative method. One should notice that in the two methods, the gravity center begins to move after a long time. Nevertheless it starts to move significantly earlier for the case with the source terms integration method. In other words, the column has moved from its initial coordinates when the pressure convergence is reached. This is crippling for example when studying interaction between a droplet and a shock wave (as seen in next subsection): the droplet must be at rest before the interaction with the shock wave. With the conservative method of the present paper, it becomes possible to consider the treatment of this kind of problem.

5.1.3. Energy conservation

Furthermore, the conservative property of the new form of the capillary effects is verified by plotting the evolution of the relative error of total mixture energy of the whole domain using wall boundary conditions (Figure 4). The energy of a closed system must be preserved. This point is verified with the conservative method but not with the source terms integration one. Moreover, for the source terms integration method, the error does not saturate and then still increases when the convergence is reached. It is also noticeable that the difference of the total mixture energy at the initialization $E(t_0)$ between source terms integration and conservative methods appears and comes from the capillary energy ε_σ which does not appear

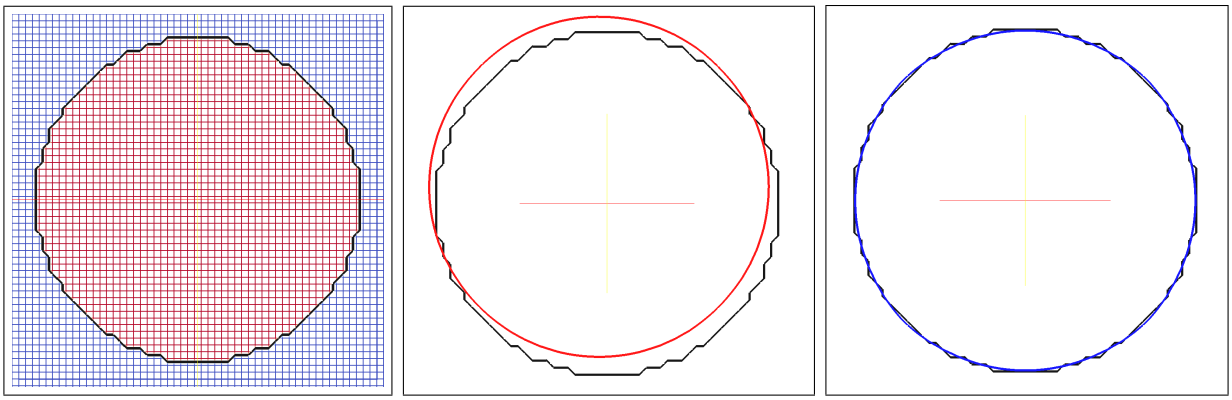

Figure 3: Magnified view of droplet contours through color function ($c = 0.5$). Initial contour together with cartesian mesh (left); Contours after convergence is reached: source terms integration method on the middle (red contour) and conservative method on the right (blue contour). With source terms integration method, the position of the droplet as already changed when convergence is reached.

in the source term form expression of the total mixture energy equation. Note that its value is here: $\varepsilon_\sigma = 2.10^7 J.m^{-3}$.

5.1.4. Pressure validation: Laplace law

The precision of the method is now analyzed regarding the Laplace law. The pressure profiles along a symmetry axis of the water column is presented in Figure 5. Converged results are presented for conservative method (blue dots), source terms integration method (red crosses) and exact solution (black lines). The new conservative method has a better accuracy then the source terms integration one.

5.1.5. Dynamic validation: square converges to circle

A square section of water column is initialized in air. The initial side of the square is $L_{square} = 20cm$. The convergence after numerous oscillations toward a circle form is presented in Figure 6. The Laplace pressure jump is verified.

5.2. Compressible validation: Shock wave interaction with a water column

The previous test cases highlight the ability of the method to deal with quasi-static capillary effects. When studying the fragmentation of droplets, the ability to deal with compressibility and shock waves must be verified. In this section, the early stages of an aerodynamic droplet breakup in a high-speed flow behind a normal shock wave are studied.

The numerical simulation takes place in two dimensions and then instead of a water droplet, a water column is retained. The dynamics of the acoustic waves are compared with experiments of Igra and Takayama [18, 19]. The cylindrical water column has a diameter $D = 6.4mm$, exposed to a shock wave of Mach number 1.3 in air (see Figure 7 for initialization sketch). The initial densities are $\rho_{air} = 1.2kg.m^{-3}$ and $\rho_{water} = 1000kg.m^{-3}$. The corresponding Weber number ($We = \rho_{air}u^2D/\sigma$) in these conditions is 3690. 2D computations are performed on cartesian meshes containing 800x800 computational cells in a physical domain of $55mm$ x $55mm$.

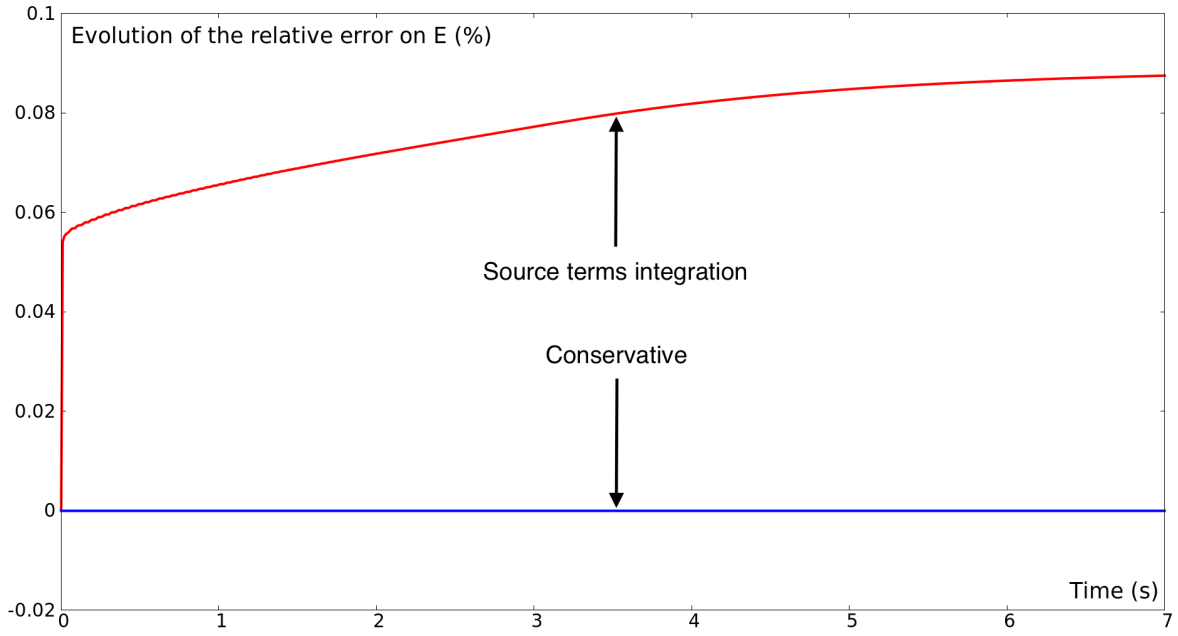

Figure 4: Evolution of the relative error of total mixture energy of the whole domain function of the physical time for the water column with wall boundary conditions. Expression for the evolution of the relative error is: $100\left(E\left(t\right)-E\left(t_0\right)\right)/E\left(t_0\right)$. Source terms integration (red) and conservative (blue) methods.

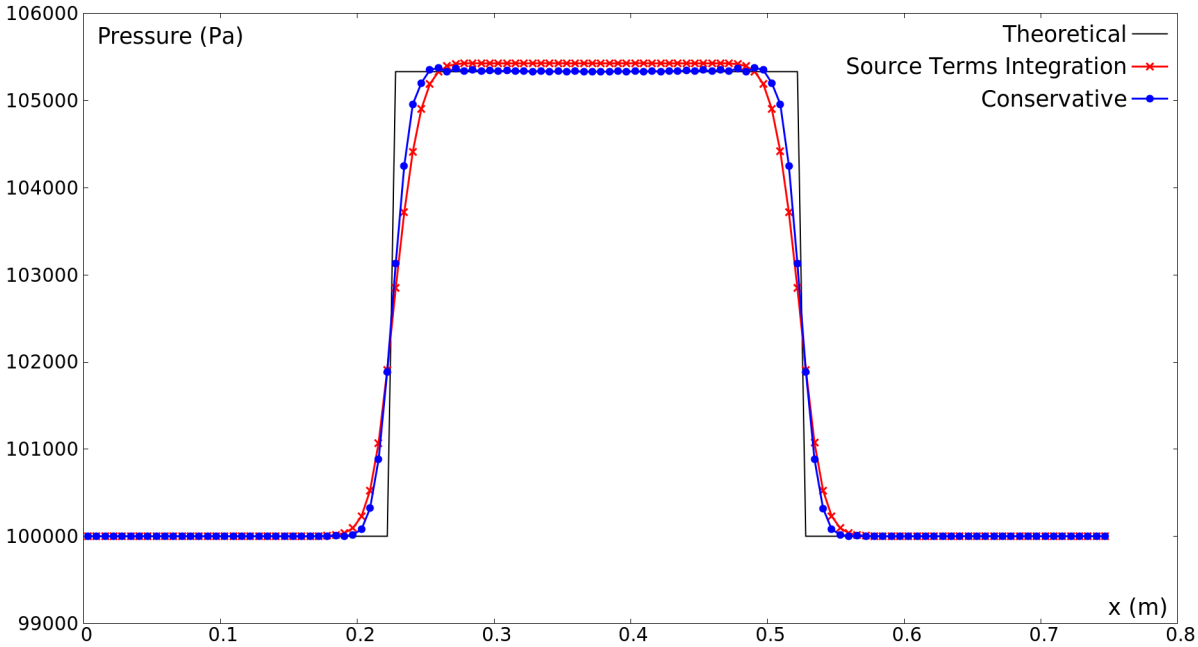

Figure 5: Pressure jump in a centered section of a steady 2D water column in air. $\sigma = 800N.m^{-1}$, $R = 0.15m$ and so $\Delta P = 5333Pa$. Theoretical (black lines) and simulations results with source terms integration (red crosses) and conservative (blue dots) methods of the capillary effects.

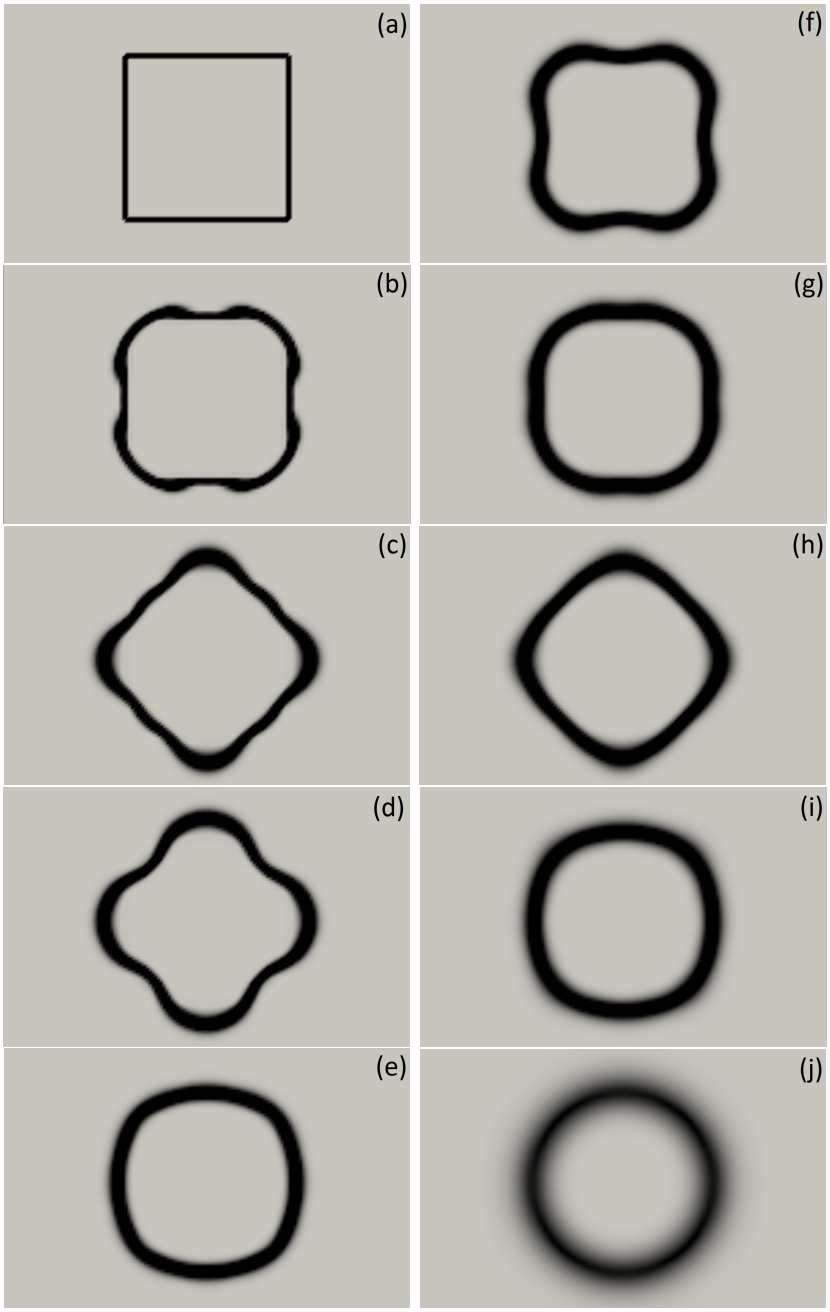

Figure 6: Schlieren images of the mixture density of 2D water under a square form in an air environment converging to a circle form. Initially $\sigma = 800N.m^{-1}$ and $L_{square} = 0.2m$. Simulation at different time instants with a mesh of 150x150: (a) initialization, (b) 5ms, (c) 15ms, (d) 20ms, (e) 30ms, (f) 35ms, (g) 45ms, (h) 50ms, (i) 105ms and (j) 3000ms.

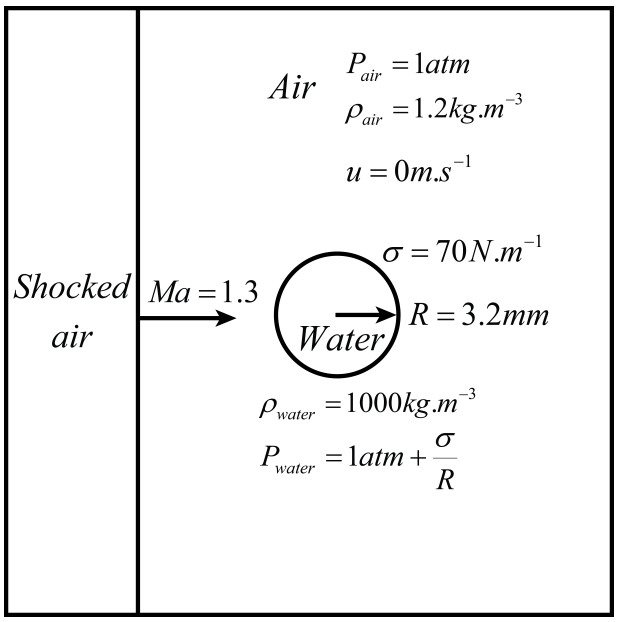

Figure 7: Sketch of the initialization for simulations treating about the shock wave on a water column.

Results are given for different time instants after the first interaction between the shock wave and the water column (Figure 8). The incident shock wave and its reflection on the water column are clearly observed through the schlieren images of the mixture density. Comparisons on the dynamics of the acoustic waves with experiments are in good agreement (Figure 9 and 10). The first filaments are observed at time $55\mu s$ in the numerical results but it is difficult to see them in experiments.

Conclusion

A new hyperbolic model treating interface problems and capillary effects has been derived together with a splitting numerical method that guarantee conservation of the mass, the momemtum and the energy. Comparison with "source terms integration method" and with experiments have shown the advantages of this new model and numerical method. The simulation of first stage of an aerodynamic breakup of a water column induced by a shock wave showed that the method will be able to treat both pressure waves interaction and capillary effects accurately in the same formulation. The next stage will be to model more complex phenomena including, in particular, viscosity effects.

Appendix: Variational principle for compressible mixtures with capillary effects

Consider a continuum characterized by the Lagrangian:

$$L = \rho \left(\frac{\|\mathbf{u}\|^2}{2} - e \right) - \sigma \|\boldsymbol{\nabla} c\|.$$

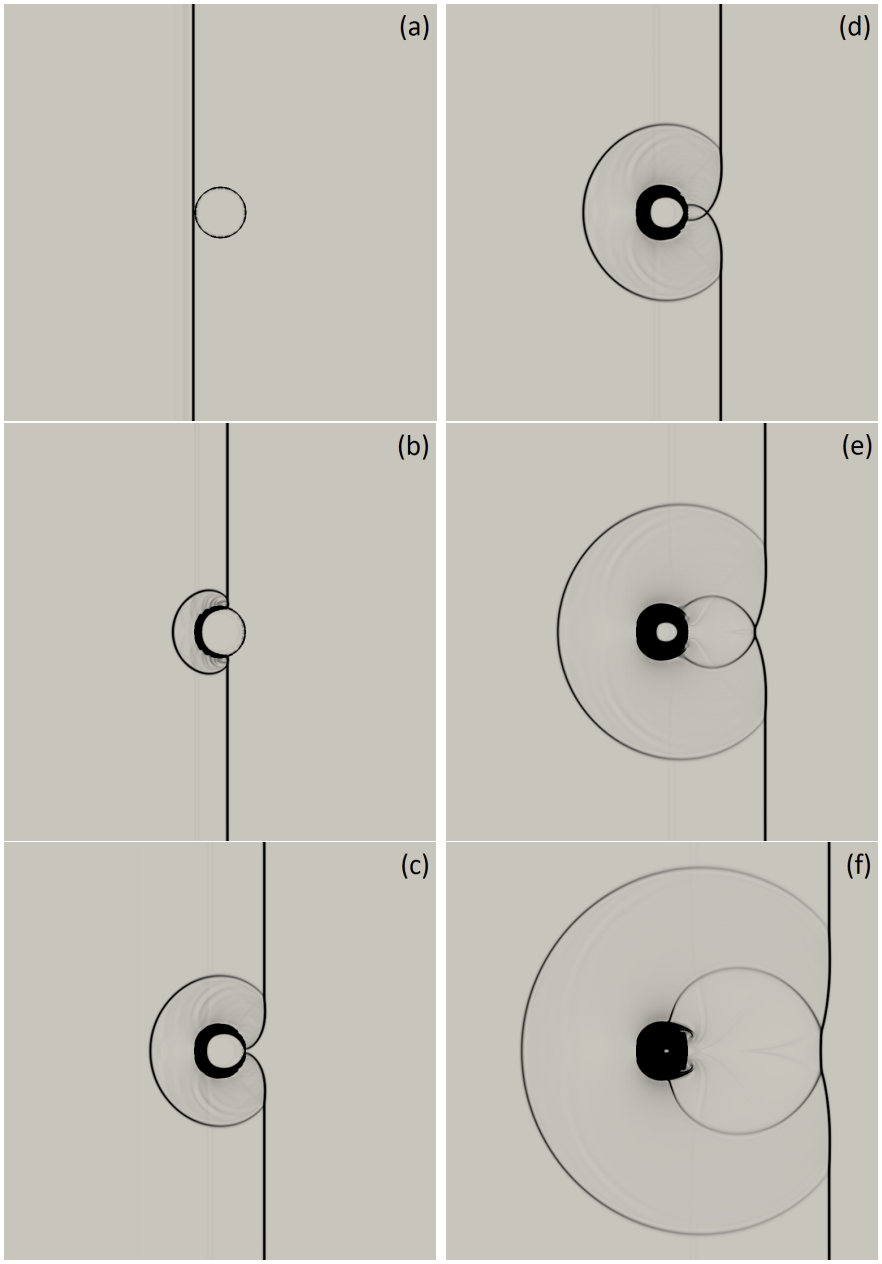

Figure 8: Early stage of the aerodynamic breakup of a water column in a high-speed airstream behind the shock wave of Mach number 1.3 in air propagating from the left to the right. 2D simulation with a mesh of 800x800 and schlieren images of the mixture density are given at the following time instants: (a) $0\mu s$, (b) $10\mu s$, (c) $20\mu s$, (d) $24\mu s$, (e) $37\mu s$ and (f) $55\mu s$.

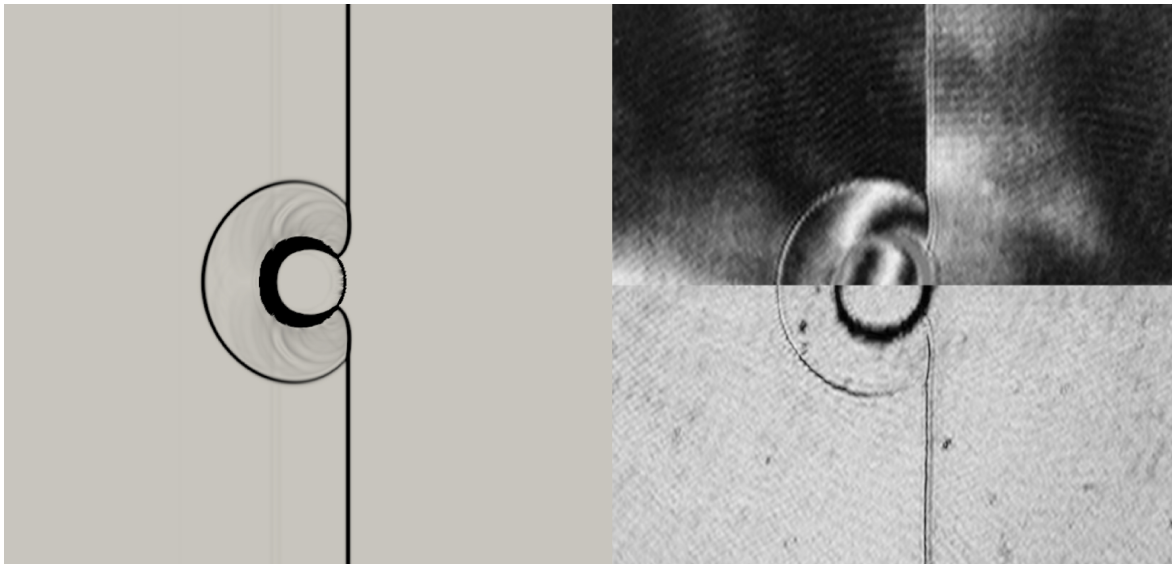

Figure 9: Early stage of the aerodynamic breakup of a water column in a high-speed airstream behind the shock wave of Mach number 1.3 in atmospheric air propagating from the left to the right. 2D simulation on the left with a mesh of 800x800 and a schlieren image of the mixture density. Experiment on the right from Igra and Takayama [19] with an interferogram on the top and an unreconstructed hologram on the bottom. Results at time instant $15\mu s$.

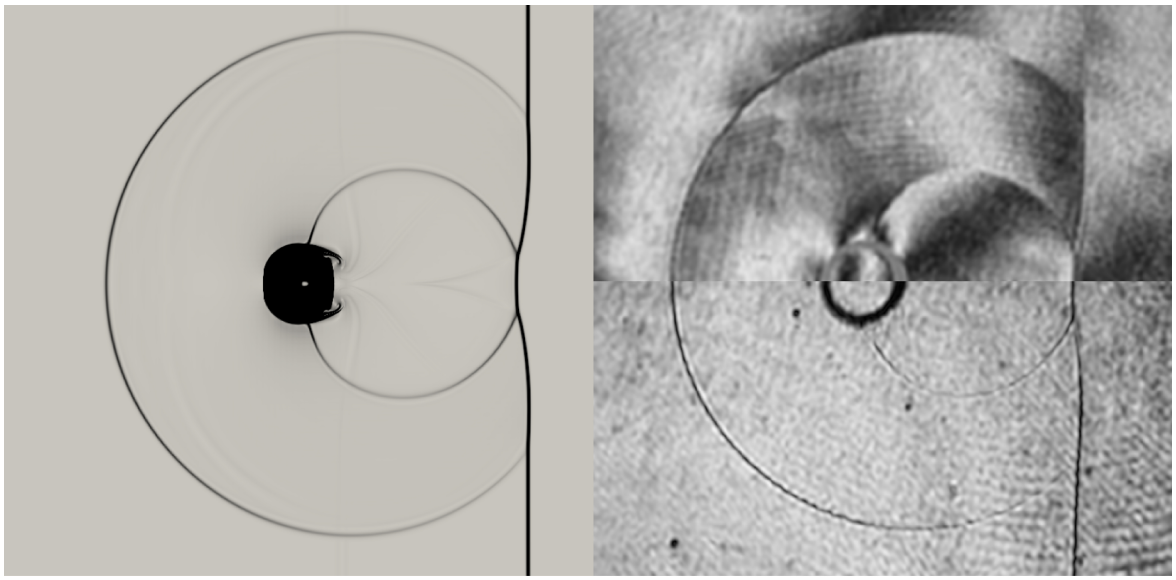

Figure 10: Early stage of the aerodynamic breakup of a water column in a high-speed airstream behind the shock wave of Mach number 1.3 in atmospheric air propagating from the left to the right. 2D simulation on the left with a mesh of 800x800 and a schlieren image of the mixture density. Experiment on the right from Igra and Takayama [19] with an interferogram on the top and an unreconstructed hologram on the bottom. Results at time instant $55\mu s$.

Here $\rho = \alpha_1\rho_1 + \alpha_2\rho_2$ is the mixture density, $e = Y_1e_1 + Y_2e_2$ is the mixture specific energy, $Y_i = \alpha_i\rho_i/\rho$ are the mass fractions, σ is the surface tension coefficient, c is the color function.

Consider the Hamilton action:

$$a = \int_{t_1}^{t_2} \int_D L dt dD, \tag{17}$$

where t_1 and t_2 are fixed time instants, and D is a material fluid volume.

The governing equations are extremal curves of the Hamilton action under the following constraints:

$$\begin{aligned}
\frac{\partial \rho}{\partial t} + \boldsymbol{\nabla}.\left(\rho \mathbf{u}\right) &= 0, \\
\frac{\partial Y_1}{\partial t} + \mathbf{u}.\boldsymbol{\nabla}\left(Y_1\right) &= 0, \\
\frac{\partial s_1}{\partial t} + \mathbf{u}.\boldsymbol{\nabla}\left(s_1\right) &= 0, \\
\frac{\partial s_2}{\partial t} + \mathbf{u}.\boldsymbol{\nabla}\left(s_2\right) &= 0, \\
\frac{\partial c}{\partial t} + \mathbf{u}.\boldsymbol{\nabla}\left(c\right) &= 0.
\end{aligned} \tag{18}$$

The Eulerian variations of the unknown variables in terms of virtual displacement $\delta\mathbf{x}$ are given by (see Gavrilyuk [12] for details):

$$\begin{aligned}
\delta\rho &= -\boldsymbol{\nabla}.\left(\rho\delta\mathbf{x}\right), \\
\delta Y_1 &= -\boldsymbol{\nabla} Y_1.\delta\mathbf{x}, \\
\delta s_1 &= -\boldsymbol{\nabla} s_1.\delta\mathbf{x}, \\
\delta s_2 &= -\boldsymbol{\nabla} s_2.\delta\mathbf{x}, \\
\delta c &= -\boldsymbol{\nabla} c.\delta\mathbf{x}, \\
\delta\mathbf{u} &= \frac{\partial \delta\mathbf{x}}{\partial t} + \frac{\partial \delta\mathbf{x}}{\partial \mathbf{x}}\mathbf{u} - \frac{\partial \mathbf{u}}{\partial \mathbf{x}}\delta\mathbf{x}.
\end{aligned}$$

Taking the variation of the Hamilton action (17) under the boundary conditions:

$$\begin{aligned}
\delta\mathbf{x}|_{\partial D} &= 0, \\
\delta\mathbf{x}|_{t=t_1} &= 0, \\
\delta\mathbf{x}|_{t=t_2} &= 0,
\end{aligned}$$

one can obtain the momentum equation:

$$\rho\left(\frac{\partial \mathbf{u}}{\partial t} + \frac{\partial \mathbf{u}}{\partial \mathbf{x}}\mathbf{u}\right) + \boldsymbol{\nabla} P = -\sigma\left(\boldsymbol{\nabla}.\mathbf{n}\right)\boldsymbol{\nabla} c,$$

with $\mathbf{n} = \boldsymbol{\nabla} c / \|\boldsymbol{\nabla} c\|$.

The equation is exactly the same as in Brackbill *et al.* [3] for the one component case. It can be written in conservative form:

$$\frac{\partial \rho \mathbf{u}}{\partial t} + \boldsymbol{\nabla}. \left(\rho \mathbf{u} \otimes \mathbf{u} + P \overline{\overline{I}} + \overline{\overline{\Omega}} \right) = 0,$$

where the capillary tensor $\overline{\overline{\Omega}}$ is given by:

$$\overline{\overline{\Omega}} = -\sigma \|\boldsymbol{\nabla} c\| \left(\overline{\overline{I}} - \mathbf{n} \otimes \mathbf{n} \right).$$

The variation of the Hamilton action with respect to the volume fraction gives as the pressure equilibrium condition:

$$P_1 = P_2 = P = \alpha_1 P_1 + \alpha_2 P_2.$$

resulting to the non-conservative equation (2) for α_1 (see Gavrilyuk [12] for details).

Using the constraints on the entropies and mass fractions of each phase, the mixture entropy equation is given by:

$$\frac{\partial s}{\partial t} + \mathbf{u}.\boldsymbol{\nabla} (s) = 0.$$

The mixture entropy, mass and momentum equations admit the following mixture total energy equation:

$$\frac{\partial \rho E}{\partial t} + \boldsymbol{\nabla}. \left((\rho E + P) \mathbf{u} \right) = - \left(\boldsymbol{\nabla}. \overline{\overline{\Omega}} \right). \mathbf{u}.$$

To transform the previous equation to a fully conservative form, the following relation is used:

$$\left(\boldsymbol{\nabla}. \overline{\overline{\Omega}} \right). \mathbf{u} = \boldsymbol{\nabla}. \left(\overline{\overline{\Omega}}. \mathbf{u} \right) - \overline{\overline{\Omega}} : \frac{\partial \mathbf{u}}{\partial \mathbf{x}},$$

where the right term still needs to be transformed. It can be developed as:

$$\sigma \left(\|\boldsymbol{\nabla} c\| \overline{\overline{I}} - \frac{\boldsymbol{\nabla} c \otimes \boldsymbol{\nabla} c}{\|\boldsymbol{\nabla} c\|} \right) : \frac{\partial \mathbf{u}}{\partial \mathbf{x}} = \sigma \left(\|\boldsymbol{\nabla} c\| \boldsymbol{\nabla}.\mathbf{u} - \left(\boldsymbol{\nabla} c. \frac{\partial \mathbf{u}}{\partial \mathbf{x}} \right). \frac{\boldsymbol{\nabla} c}{\|\boldsymbol{\nabla} c\|} \right). \tag{19}$$

Using the material derivative equation of $\|\boldsymbol{\nabla} c\|$:

$$\frac{d\|\boldsymbol{\nabla} c\|}{dt} = \frac{d\boldsymbol{\nabla} c}{dt}. \frac{\boldsymbol{\nabla} c}{\|\boldsymbol{\nabla} c\|}, \tag{20}$$

with the material derivative operator $d(\cdot)/dt = \partial(\cdot)/\partial t + \mathbf{u}.\boldsymbol{\nabla}(\cdot)$ and the Schwarz theorem, we have:

$$\frac{d\boldsymbol{\nabla} c}{dt} = \boldsymbol{\nabla} \left(\frac{dc}{dt} \right) - \boldsymbol{\nabla} c. \frac{\partial \mathbf{u}}{\partial \mathbf{x}}. \tag{21}$$

Hence with equations (18) and (21), equation (20) is rewritten as:

$$\frac{d\|\boldsymbol{\nabla} c\|}{dt} = - \left(\boldsymbol{\nabla} c. \frac{\partial \mathbf{u}}{\partial \mathbf{x}} \right). \frac{\boldsymbol{\nabla} c}{\|\boldsymbol{\nabla} c\|}.$$

Thus relation (19) is now developed as:

$$\sigma\left(\|\boldsymbol{\nabla} c\|\overline{\overline{I}} - \frac{\boldsymbol{\nabla} c \otimes \boldsymbol{\nabla} c}{\|\boldsymbol{\nabla} c\|}\right) : \frac{\partial \mathbf{u}}{\partial \mathbf{x}} = \sigma\left(\|\boldsymbol{\nabla} c\| \boldsymbol{\nabla}.\mathbf{u} + \frac{d\|\boldsymbol{\nabla} c\|}{dt}\right)$$

$$= \frac{\partial \sigma \|\boldsymbol{\nabla} c\|}{\partial t} + \boldsymbol{\nabla}.\left(\sigma \|\boldsymbol{\nabla} c\| \mathbf{u}\right).$$

Finally, the energy conservation law is:

$$\frac{\partial \rho E + \varepsilon_\sigma}{\partial t} + \boldsymbol{\nabla}.\left(\left(\rho E + \varepsilon_\sigma + P\right)\mathbf{u} + \overline{\overline{\Omega}}.\mathbf{u}\right) = 0,$$

with the capillary energy term $\varepsilon_\sigma = \sigma\|\boldsymbol{\nabla} c\|$.

Acknowledgments

Authors are particularly grateful to Dan Igra for providing experimental data and to Sarah Hank for fruitful discussions.

References

[1] R. Abgrall and S. Karni. Computations of compressible mutlifluids. *Journal of Computational Physics*, 169(2):594–623, 2001.

[2] G. Allaire, S. Clerc, and S. Kokh. A five-equation model for the simulation of interfaces between compressible fluids. *J. Comp. Phys.*, 181:577–616, 2002.

[3] J. Brackbill, D. Kothe, and C. Zemach. A continuum method for modelling surface tension. *Journal of Computational Physics*, 100:335–354, 1992.

[4] A. Chauvin, E. Daniel, A. Chinnayya, J. Massoni, and G. Jourdan. Shock waves in sprays: numerical study of secondary atomization and experimental comparison. *Shock Waves*, pages 1–13, 2015.

[5] A. Chauvin, G. Jourdan, E. Daniel, L. Houas, and R. Tosello. Experimental investigation of the propagation of a planar shock wave through a two-phase gas-liquid medium. *Physics of Fluids (1994-present)*, 23(11):113301, 2011.

[6] S. Chen and G.D. Doolen. Lattice boltzmann method for fluid flows. *Annual review of fluid mechanics*, 30(1):329–364, 1998.

[7] B.M. Devassy, C. Habchi, and E. Daniel. Atomization modelling of liquid jets using a two-surface-density approach. *Atomization and Sprays*, 25(1):47–80, 2015.

[8] O.G. Engel. Fragmentation of waterdrops in the zone behind an air shock. *J. Res. Natl. Bur. Stand*, 60(3):245–280, 1958.

[9] N. Favrie and S.L. Gavrilyuk. Diffuse interface model for compressible fluid–compressible elastic–plastic solid interaction. *Journal of Computational Physics*, 231(7):2695–2723, 2012.

[10] N. Favrie and S.L. Gavrilyuk. Dynamic compaction of granular materials. *Proceedings of the Royal Society of London A: Mathematical, Physical and Engineering Sciences*, 469(2160):20130214, 2013.

[11] N. Favrie, S.L. Gavrilyuk, and S. Ndanou. A thermodynamically compatible splitting procedure in hyperelasticity. *Journal of Computational Physics*, 270:300–324, 2014.

[12] S.L. Gavrilyuk. *Multiphase flow modeling via Hamilton's principle. In the book: F. Dell'Isola and S.L. Gavrilyuk, Eds. Variational models and methods in solid and fluid mechanics, CISM Courses and Lectures*, volume 535. Springer, 2012.

[13] S.L. Gavrilyuk and R. Saurel. Rankine–hugoniot relations for shocks in heterogeneous mixtures. *Journal of Fluid Mechanics*, 575:495–507, 2007.

[14] S.K. Godunov. A finite difference method for numerical computation of discontinuous solutions of the equations of fluid dynamics. *Math Sb.*, 47:357–393, 1959.

[15] D. Gueyffier, L. Li, A. Nadim, R. Scardovelli, and S. Zaleski. Volume-of-fluid interface tracking with smoothed surface stress methods for three-dimensional flows. *Journal of Computational Physics*, 152:423–456, 1999.

[16] L-P. Hsiang and G.M. Faeth. Near-limit drop deformation and secondary breakup. *International Journal of Multiphase Flow*, 18(5):635–652, 1992.

[17] D. Igra and K. Takayama. Investigation of aerodynamic breakup of a cylindrical water droplet. *Atomization and Sprays*, 11(2):167–185, 2001.

[18] D. Igra and K. Takayama. Numerical simulation of shock wave interaction with a water column. *Shock Waves*, 11(3):219–228, 2001.

[19] D. Igra and K. Takayama. A study of shock wave loading on a cylindrical water column. *Report of the Institute of Fluid Science, Tohoku University*, 13:19–36, 2001.

[20] D.D. Joseph, J. Belanger, and G.S. Beavers. Breakup of a liquid drop suddenly exposed to a high-speed airstream. *International Journal of Multiphase Flow*, 25(6):1263–1303, 1999.

[21] A. Kapila, R. Menikoff, J. Bdzil, S. Son, and D. Stewart. Two-phase modeling of DDT in granular materials: Reduced equations. *Physics of Fluids*, 13:3002–3024, 2001.

[22] G. Layes and O. Le Metayer. Quantitative numerical and experimental studies of the shock accelerated heterogeneous bubbles motion. *Physics of Fluids*, 19(042105), 2007.

[23] S. Le Martelot, R. Saurel, and B. Nkonga. Towards the direct numerical simulation of nucleate boiling flows. *International Journal of Multiphase Flow*, 66:62–78, 2014.

[24] J. Massoni, R. Saurel, B. Nkonga, and R. Abgrall. Proposition de methodes et modeles Euleriens pour les problemes a interfaces entre fluides compressibles en presence de transfert de chaleur. *Int. J. Heat and Mass Transfer*, 45:1287–1307, 2002.

[25] J.C. Meng and T. Colonius. Numerical simulations of the early stages of high-speed droplet breakup. *Shock Waves*, pages 1–16, 2014.

[26] A. Murrone and H. Guillard. Behavior of upwind scheme in the low mach number limit: Iii. preconditioned dissipation for a five equation two phase model. *Computers & Fluids*, 37(10):1209–1224, 2008.

[27] S. Ndanou, N. Favrie, and S.L. Gavrilyuk. Criterion of hyperbolicity in hyperelasticity in the case of the stored energy in separable form. *Journal of Elasticity*, 115(1):1–25, 2014.

[28] S. Osher and R. Fedkiw. Level set methods: An overview and some recent results. *Journal of Computational Physics*, 169:463–502, 2001.

[29] S. Osher and R. Fedkiw. *Level set methods and dynamic implicit surfaces*, volume 153. Springer Science & Business Media, 2006.

[30] G. Périgaud and R. Saurel. A compressible flow model with capillary effects. *J. Comp. Phys.*, 209:139–178, 2005.

[31] F. Petitpas, J. Massoni, R. Saurel, E. Lapebie, and L. Munier. Diffuse interface models for high speed cavitating underwater systems. *Int. J. of Multiphase Flows*, 35(8):747–759, 2009.

[32] F. Petitpas, R. Saurel, E. Franquet, and A. Chinnayya. Modelling detonation waves in condensed energetic materials: Multiphase CJ conditions and multidimensional computations. *Shock waves*, 19(5):377–401, 2009.

[33] M. Pilch and C.A. Erdman. Use of breakup time data and velocity history data to predict the maximum size of stable fragments for acceleration-induced breakup of a liquid drop. *International Journal of Multiphase Flow*, 13(6):741–757, 1987.

[34] J.J. Quirk and S. Karni. On the dynamics of a shock–bubble interaction. *Journal of Fluid Mechanics*, 318:129–163, 1996.

[35] R. Saurel and R. Abgrall. A simple method for compressible multifluid flows. *SIAM J. Sci. Comp.*, 21(3):1115–1145, 1999.

[36] R. Saurel, S.L. Gavrilyuk, and F. Renaud. A multiphase model with internal degrees of freedom: Application to shock-bubble interaction. *Journal of Fluid Mechanics*, 495:283–321, 2003.

[37] R. Saurel, F. Petitpas, and R. Abgrall. Modelling phase transition in metastable liquids: application to cavitating and flashing flows. *Journal of Fluid Mechanics*, 607:313–350, 2008.

[38] R. Saurel, F. Petitpas, and R.A. Berry. Simple and efficient relaxation methods for interfaces separating compressible fluids, cavitating flows and shocks in multiphase mixtures. *Journal of Computational Physics*, 228(5):1678–1712, 2009.

[39] M. Sussman, P. Smereka, and S. Osher. A level set approach for computing solutions to incompressible two-phase flow. *Journal of Computational Physics*, 114(1):146–159, 1994.

[40] G. Tryggvason, B. Bunner, A. Esmaeeli, D. Juric, N. Al-Rawahi, W. Tauber, J. Han, S. Nas, and Y-J. Jan. A front-tracking method for the computations of multiphase flow. *Journal of Computational Physics*, 169(2):708–759, 2001.

[41] P. Welch and P. Boyle. New turbines to enable efficient geothermal power plants. *Geothermal Resources Council Transactions*, 33:765–772, 2009.

[42] A. Wierzba and K. Takayama. Experimental investigation on liquid droplet breakup in a gas stream. *Rept. Inst. High Speed Mech.(Tohoku Univ.)*, 53(382):1–99, 1987.

[43] A.B. Wood. A textbook of sound. *G. Bell and Sons LTD, London*, 1930.

[44] J. Yang, T. Kubota, and E.E. Zukoski. A model for characterization of a vortex pair formed by shock passage over a light-gas inhomogeneity. *Journal of Fluid Mechanics*, 258:217–244, 1994.